Cell

Derepression of a Neuronal Inhibitor due to miRNA Dysregulation in a Schizophrenia-Related Microdeletion

Bin Xu,[1,3,5] Pei-Ken Hsu,[3,4,5] Kimberly L. Stark,[1,3] Maria Karayiorgou,[1,*] and Joseph A. Gogos[2,3,*]
[1]Department of Psychiatry
[2]Department of Neuroscience
College of Physicians and Surgeons, Columbia University, 1051 Riverside Drive, New York, NY 10032, USA
[3]Department of Physiology and Cellular Biophysics, College of Physicians and Surgeons
[4]Integrated Program in Cellular, Molecular, and Biophysical Studies
Columbia University, 630 West 168th Street, New York, NY 10032, USA
[5]These authors contributed equally to this work
*Correspondence: mk2758@columbia.edu (M.K.), jag90@columbia.edu (J.A.G.)
http://dx.doi.org/10.1016/j.cell.2012.11.052

SUMMARY

22q11.2 microdeletions result in specific cognitive deficits and schizophrenia. Analysis of *Df(16)A*$^{+/-}$ mice, which model this microdeletion, revealed abnormalities in the formation of neuronal dendrites and spines, as well as altered brain microRNAs. Here, we show a drastic reduction of *miR-185*, which resides within the 22q11.2 locus, to levels more than expected by a hemizygous deletion, and we demonstrate that this reduction alters dendritic and spine development. *miR-185* represses, through an evolutionarily conserved target site, a previously unknown inhibitor of these processes that resides in the Golgi apparatus and shows higher prenatal brain expression. Sustained derepression of this inhibitor after birth represents the most robust transcriptional disturbance in the brains of *Df(16)A*$^{+/-}$ mice and results in structural alterations in the hippocampus. Reduction of *miR-185* also has milder age- and region-specific effects on the expression of some Golgi-related genes. Our findings illuminate the contribution of microRNAs in psychiatric disorders and cognitive dysfunction.

INTRODUCTION

The identification of a widespread role of chromosomal microdeletions and microduplications (copy number variants or CNVs) in determining susceptibility to psychiatric disorders such as schizophrenia (SCZ), as well as neurodevelopmental disorders such as autism and intellectual disability, represents a shift in our understanding of the genetic architecture of these disorders and highlights the pervasive contribution of rare and highly penetrant structural mutations (Karayiorgou et al., 1995; Morrow, 2010; Rodriguez-Murillo et al., 2012). Along these lines, a strong link has been established between microdeletions in chromosome 22q11.2, cognitive dysfunction and psychiatric disorders, especially SCZ (Karayiorgou et al., 1995, 2010; Xu et al., 2008). Understanding how the genes disrupted by this deletion contribute to the ensuing psychiatric and cognitive phenotypes will provide important mechanistic insights and guide analysis of other pathogenic mutations (Arguello and Gogos, 2006, 2010, 2012; International Schizophrenia Consortium, 2008; Karayiorgou et al., 2010).

By using chromosomal engineering, we generated a mouse model carrying a hemizygous 1.3 Mb chromosomal deficiency on mouse chromosome 16 (*Df(16)A*), which is syntenic to the 1.5 Mb 22q11.2 microdeletion (Stark et al., 2008). Analysis of *Df(16)A*$^{+/-}$ mice showed abnormalities in dendritic morphogenesis and formation of dendritic spines of hippocampal pyramidal neurons both in culture and in vivo (Mukai et al., 2008; Stark et al., 2008). Such changes may account, at least in part, for the regional decreases in gray matter volumes observed in some 22q11.2 deletion carriers (Bearden et al., 2009; Chow et al., 2002) and may ultimately lead to altered information processing.

Analysis of the *Df(16)A*$^{+/-}$ strain also provided compelling evidence that the 22q11.2 microdeletion results in abnormal processing of brain microRNAs (miRNAs), a class of small noncoding RNAs that regulate the stability and translation of mRNAs (Fineberg et al., 2009; Kosik, 2006; Schratt, 2009; Xu et al., 2010), implicating miRNA dysregulation in the pathogenesis of psychiatric disorders and cognitive dysfunction. One gene disrupted by the 22q11.2 microdeletion is *DGCR8*, a component of the "microprocessor" complex that is essential for miRNA production (Tomari and Zamore, 2005). *Dgcr8* haploinsufficiency results in the downregulation of a specific subset of mature miRNAs and contributes to alterations found in *Df(16)A*$^{+/-}$ mice (Fénelon et al., 2011; Stark et al., 2008). miRNA dysregulation likely accounts for a fraction of the transcript misexpression in the brains of *Df(16)A*$^{+/-}$ mice (Stark et al., 2008), but direct targets have not been reported. Here, we highlight an important component of this dysregulation and identify a previously uncharacterized gene with prenatal expression bias as a major

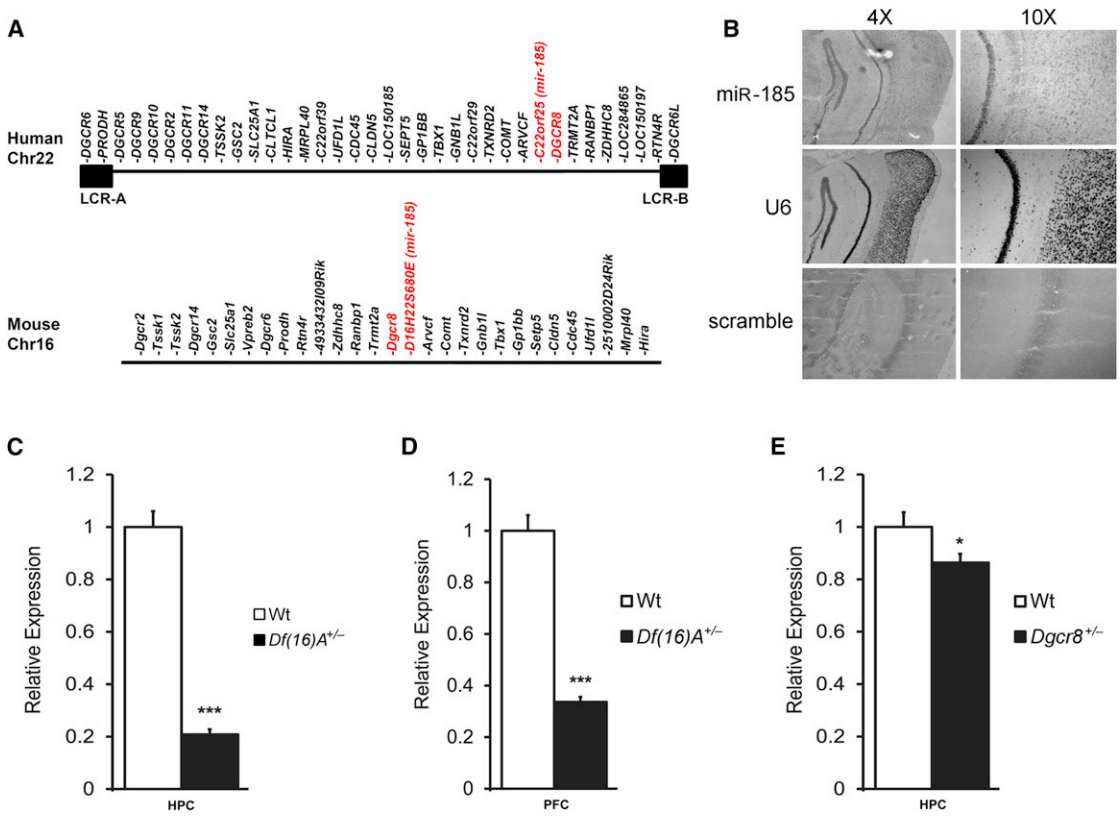

Figure 1. Drastic Reduction of *mir-185* Expression in *Df(16)A*$^{+/-}$ Mice

(A) Schematic diagram showing the 1.5 Mb 22q11.2 critical region and the syntenic mouse locus. The 1.5 Mb deletion is mediated by low copy repeat sequences LCR-A and LCR-B (illustrated as black boxes). *Dgcr8* and *miR-185* (hosted in the intron of the *22orf25* gene in human and the *D16H22S680E* gene in mouse) are highlighted in red. Chr22, chromosome 22; Chr16, chromosome 16.

(B) Expression of *miR-185* mRNA in HPC and cortex as shown by in situ hybridization in coronal brain sections using an antisense miR-185 probe. An antisense U6 probe and a scramble probe were used as positive and negative controls, respectively. Images were taken at either 4× (left) or 10× (right) magnification.

(C–E) *miR-185* expression levels in HPC (C) or PFC (D) of *Df(16)A*$^{+/-}$ (n = 7 for mutant, n = 9 for WT) and in HPC (E) of *Dgcr8*$^{+/-}$ (n = 10 for mutant and WT), as assayed by qRT-PCR. Expression levels in mutant mice were normalized to their respective WT littermates.

Results are expressed as mean ±SEM. *p < 0.05, **p < 0.01, and ***p < 0.001 (Student's t test). See also Figure S1.

miRNA target mediating the effects of the 22q11.2 microdeletion on neuronal maturation and connectivity.

RESULTS

A Drastic Reduction of *miR-185* Levels in *Df(16)A*$^{+/-}$ Mice

Studies in the *Df(16)A*$^{+/-}$ mouse strain have shown that the 22q11.2 microdeletion results in abnormal processing of a specific subset of brain miRNAs due to the removal of one copy of the *Dgcr8* gene causing a decrease in its expression in the adult brain (Stark et al., 2008) as well as in early development (Figure S1A available online). It is noteworthy that, in addition to *Dgcr8*, the 22q11.2 microdeletion and the equivalent mouse deficiency remove one copy of a miRNA gene (*miR-185*) located within the minimal 1.5 Mb 22q11.2 critical region (Figure 1A). In situ hybridization assays indicated that *miR-185* is expressed in several brain regions such as hippocampus (HPC) and cortex (Figure 1B). qRT-PCR analysis showed that expression of *miR-185* is dramatically reduced by ~70%–80% in both HPC ($p < 10^{-6}$) and prefrontal cortex (PFC; $p < 10^{-11}$) of adult *Df(16)A*$^{+/-}$ mice as compared to wild-type (WT) littermates (Figures 1C and 1D). This reduction was also observed at earlier developmental stages (embryonic day 17 [E17] and postnatal day 6 [P6]) (Figure S1B). *miR-185* also showed a more modest decrease in *Dgcr8*$^{+/-}$ mice (~20% in HPC; $p < 0.05$; Figure 1E), suggesting that the severe reduction of mature miR-185 expression in *Df(16)A*$^{+/-}$ mice may be due to a combined effect of hemizygosity of the *miR-185* gene and impaired maturation of the pri-mir-185 transcript produced from the remaining copy, due to the reduction in Dgcr8 levels. Such a large reduction in expression of a resident gene to levels greater than expected by the 50% decrease in gene dosage is unique among genes affected by the 22q11.2 microdeletion.

A Primary Transcriptional Consequence of 22q11.2 Genomic Loss

Previous microarray analysis of adult *Df(16)A*$^{+/-}$ mice revealed genome-wide alterations of transcriptional programs in the HPC and PFC (Stark et al., 2008). We extended expression

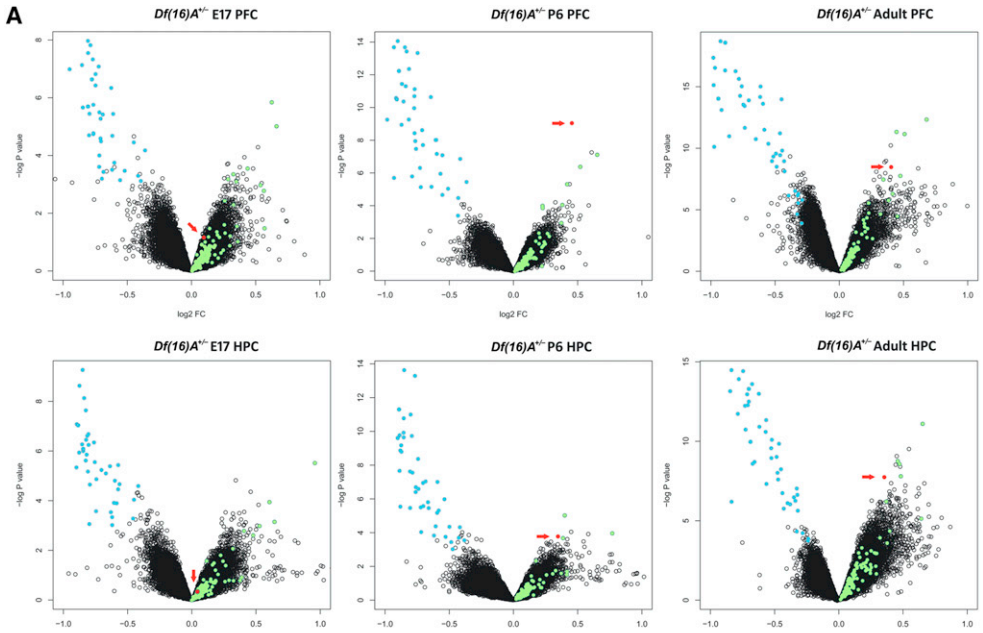

B

E17 PFC			P6 PFC			Adult PFC		
AffyID	Symbols	*P*-Value	AffyID	Symbols	*P*-Value	AffyID	Symbols	*P*-Value
1450625_at	Col5a2	1.15E-04	1424038_a_at	2310044H10Rik	9.08E-10	1455326_at	Clec16a	1.38E-09
1430644_at	Wbscr25	1.92E-04	1428021_at	Mccc2	5.82E-05	1424038_a_at	2310044H10Rik	3.40E-09
1419147_at	Rec8	4.30E-04	1430976_a_at	Mrpl9	6.26E-05	1456488_at	Wdr33	4.36E-09
1419028_at	Arpp21	4.49E-04	1438967_x_at	Amhr2	9.71E-05	1428208_at	Bcl7a	1.06E-08
1427083_a_at	Map4k5	4.79E-04	1427962_at	Ccdc102a	1.03E-04	1437125_at	Camk2a	3.73E-08
1440240_at	Npb	6.16E-04	1437236_a_at	Zfp110	1.49E-04	1439661_at	Slc16a14	3.76E-08
1421648_at	Nlgn1	6.30E-04	1451688_s_at	Cant1	1.76E-04	1426446_at	6430548M08Rik	6.03E-08
1424659_at	Slit2	8.03E-04	1453380_a_at	Xrcc6bp1	1.77E-04	1458870_x_at	Mycbp2	1.04E-07
1458119_at	Slc25a27	8.84E-04	1420117_at	Golph3	2.04E-04	1452322_a_at	Brwd1	1.32E-07
1449914_at	Ribc1	9.42E-04	1431678_at	4930556N08Rik	2.32E-04	1450661_x_at	Nfic	1.61E-07

E17 HPC			P6 HPC			Adult HPC		
AffyID	Symbols	*P*-Value	AffyID	Symbols	*P*-Value	AffyID	Symbols	*P*-Value
1450625_at	Col5a2	4.40E-05	1460613_x_at	Gh	8.98E-05	1455326_at	Clec16a	8.58E-10
1460245_at	Klrd1	2.84E-04	1424038_a_at	2310044H10Rik	1.68E-04	1423125_at	Dclk1	2.98E-09
1460451_at	Tmem52	2.96E-04	1418547_at	Tfpi2	2.42E-04	1425690_at	B3gat1	3.94E-09
1453816_at	Nsa2	4.81E-04	1460471_at	Ooep	3.33E-04	1424038_a_at	2310044H10Rik	1.81E-08
1420170_at	Myh9	5.38E-04	1418541_at	Cenpo	3.44E-04	1441312_at	Cnnm1	4.33E-08
1434423_at	Gulp1	5.72E-04	1427202_at	4833442J19Rik	4.12E-04	1449931_at	Cpeb4	4.44E-08
1442160_at	Fam19a3	5.73E-04	1438624_x_at	Hs3st2	4.66E-04	1421200_at	Dlg2	9.01E-08
1422263_at	Bdkrb2	8.09E-04	1421298_a_at	Hipk1	4.75E-04	1421339_at	Extl3	1.10E-07
1416529_at	Emp1	8.99E-04	1449191_at	Wfdc12	4.87E-04	1431254_at	Kbtbd11	1.40E-07
1418710_at	Cd59a	9.23E-04	1454576_at	A230102O21Rik	5.02E-04	1452742_at	Trak1	1.45E-07

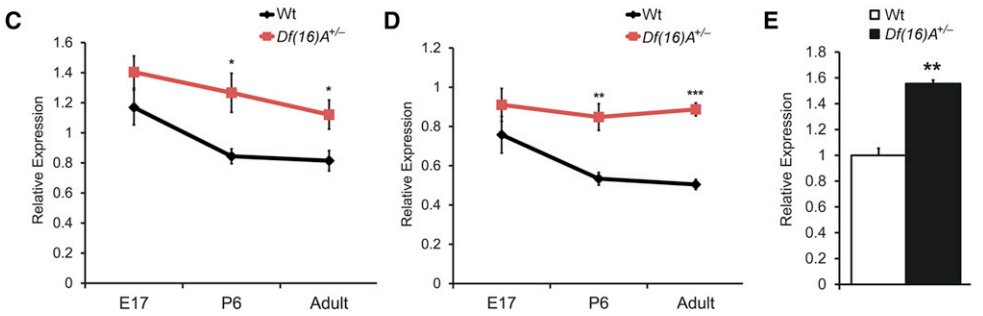

Figure 2. *2310044H10Rik* Is Robustly Upregulated in the Brain of *Df(16)A*$^{+/-}$ Mice

(A) Changes in gene expression in the PFC (upper panel) or HPC (lower panel) of *Df(16)A*$^{+/-}$ and WT littermate control mice at E16, P6, and adulthood (n = 10 each group). Volcano plot of the p values and the corresponding relative expression of each gene are shown. Light blue dots indicate genes within *Df(16)A* deficiency, light green dots indicate upregulated miRNA-containing transcripts, and red dots indicate probe sets representing *Mirta22*.

(B) Top ten protein-encoding genes that show significant upregulation in the PFC (upper panel) or HPC (lower panel) of *Df(16)A*$^{+/-}$ and WT littermate mice at E16, P6, and adulthood. *Mirta22* is highlighted in red.

(legend continued on next page)

profile analysis of these two brain regions to two earlier developmental stages, E17 and P6. Only one gene, *2310044H10Rik*, was consistently significantly upregulated (in at least two of the three developmental stages examined and in at least one of the two brain areas tested). Indeed, *2310044H10Rik* was among the top upregulated genes in both postnatal stages examined (Figures 2A and 2B). Notably, no significant difference in *2310044H10Rik* expression was found in either frontal cortex or HPC at E17 (Figures 2A and 2B). Importantly, there is no known miRNA within or surrounding this genomic locus, suggesting that the upregulation is not due to impaired processing of overlapping pri-miRNA transcripts.

In independent experiments, we attempted to distinguish primary versus secondary gene targets of the 22q11.2 microdeletion by looking for genes whose expression changes in opposite direction as a result of genomic losses or gains in this locus. Such genes are likely to represent primary targets and direct transcriptional readouts of the underlying copy number imbalances (Chahrour et al., 2008). We compared the PFC and HPC gene expression profiles in mice carrying a deletion or duplication at the 22q11.2 syntenic mouse locus using as reference compound heterozygous mice balanced for copy number (see Extended Experimental Procedures; Figure S2). We identified a number of inversely altered transcripts in either PFC or HPC ($p < 0.001$; Extended Experimental Procedures; Table S1), in addition to the transcripts from the 22q11.2 region. As expected, the majority of the identified transcripts are pri-miRNA forms. Only 12 transcripts were significantly misregulated in a reciprocal manner in both PFC and HPC (Table S2). Among them, *2310044H10Rik* is the only gene with protein-coding potential.

Taken together, our expression profiling highlighted the misregulation of *2310044H10Rik* as a major consequence of the 22q11.2 genomic imbalances at the transcriptome level. We confirmed the pattern of *2310044H10Rik* upregulation in both PFC and HPC by TaqMan qRT-PCR (PFC: E17, 20%, $p = 0.24$; P6, 59%, $p < 0.01$; Adult, 76%, $p < 10^{-6}$; HPC: E17, 20%, $p = 0.16$; P6, 50%, $p < 0.05$; Adult, 38%, $p < 0.05$; Figures 2C and 2D). This analysis revealed a profile of temporal regulation with prenatal expression bias where levels of *2310044H10Rik* rapidly decline during the first week after birth and remain constantly low thereafter, as well as a corresponding pattern of misregulation in *Df(16)A*$^{+/-}$ mice where prenatally elevated expression persists throughout postnatal and adult life. Increased brain expression of *2310044H10Rik* is recapitulated in *Df(16)A*$^{+/-}$ primary neurons (Figure 2E).

2310044H10Rik Is a Major Downstream Effector of miRNA Dysregulation

Notably, *2310044H10Rik* mRNA levels were also elevated in *Dgcr8*$^{+/-}$ mice (HPC: 30%, $p < 0.05$; PFC: 24%, $p < 0.05$; Figure S3A), suggesting that upregulation may be due to miRNA dysregulation. Indeed, two miRNA target site prediction programs, TargetScan (Grimson et al., 2007) and mirDB (Wang, 2008), report that the 3′ UTR of *2310044H10Rik* contains binding sites of miRNAs shown to be affected in *Df(16)A*$^{+/-}$ mice by microarray profiling (Stark et al., 2008). Specifically, mirDB predicted five such miRNAs with binding sites in the 3′ UTR of *2310044H10Rik* including miR-185 and miR-485, whereas TargetScan predicted 13 miRNA sites, including sites for miR-185, miR-485, miR-491, and miR-224. Notably, both programs predicted sites for miR-185 and miR-485 (Figure 3A, red rectangles).

Because increased brain expression of *2310044H10Rik* is recapitulated in *Df(16)A*$^{+/-}$ primary neurons (Figure 2E), we first used primary neurons to determine whether endogenous *2310044H10Rik* expression is actually under the control of miR-185. To examine the effect of miR-185 overexpression on *2310044H10Rik* level, we introduced into primary neuronal cultures a miRNA precursor mimic (“pre-mir-185”), which is processed into mature miRNA, or a scramble precursor (“prescramble”) with no homology to the mouse genome, which serves as a control for nonspecific effects of small RNA expression. Twenty-four hours posttransfection, there was a decrease in the levels of *2310044H10Rik* in pre-mir-185-transfected neurons when compared to prescramble-transfected neurons ($p < 0.01$; Figure 3B). In a complementary experiment, introduction of an anti-miR-185 LNA oligo or a scramble control oligo resulted in an increase of *2310044H10Rik* mRNA levels in anti-miR-185-transfected cells when compared to scramble-transfected cells ($p < 0.05$; Figure 3C). Taken together, these results confirm that *2310044H10Rik* expression in primary neurons is under the repressive control of miR-185. Essentially identical results were obtained when *2310044H10Rik* expression was assayed in N18 cells (Figures 3D and 3E). Therefore, we used this cell line to further characterize the miR-185-mediated inhibition.

To test whether the inhibition of miR-185 on *2310044H10Rik* expression is 3′ UTR dependent as predicted by TargetScan and mirDB (see above), *2310044H10Rik* 3′ UTR-fused luciferase reporter genes were cotransfected with either pre-mir-185 mimic or prescramble into N18 cells. Although prescramble did not affect the reporter activity, introduction of pre-mir-185 mimic led to a dramatic decrease of luciferase activity as compared to the prescramble control ($p < 0.001$ for all pre-mir-185 concentrations used; Figure 3F). To investigate whether miR-185-mediated repression is specific and operates directly via the two binding sites predicted by TargetScan (Figure 3A), we engineered luciferase reporters carrying mutated versions of *2310044H10Rik* 3′ UTR with either individual or both miR-185 binding sites mutated (Mut1:Site 1 mutant; Mut2:Site 2 mutant; Mut1&2:Site 1 and 2 mutants, see Extended Experimental Procedures). The pre-mir-185 mimic significantly reduced the luciferase activity of the WT reporter to ~25% relative to a control reporter without 3′ UTR, whereas it reduced the luciferase activities of the Mut1 and Mut2 reporters to 80% ($p < 0.01$) and 33%

(C and D) Temporal expression of *2310044H10Rik* (*Mirta22*) in the PFC (C) and HPC (D) of *Df(16)A*$^{+/-}$ and WT littermate mice as monitored by qRT-PCR (n = 9–10 for each group).

(E) Increased expression of endogenous *2310044H10Rik* (*Mirta22*) in DIV9 hippocampal neurons isolated from *Df(16)A*$^{+/-}$ animals as assayed by qRT-PCR (n = 3 each genotype). Expression levels in mutant neurons were normalized to WT neurons.

Results are expressed as mean ±SEM. *$p < 0.05$, **$p < 0.01$, and ***$p < 0.001$ (Student’s t test). See also Figure S2 and Tables S1 and S2.

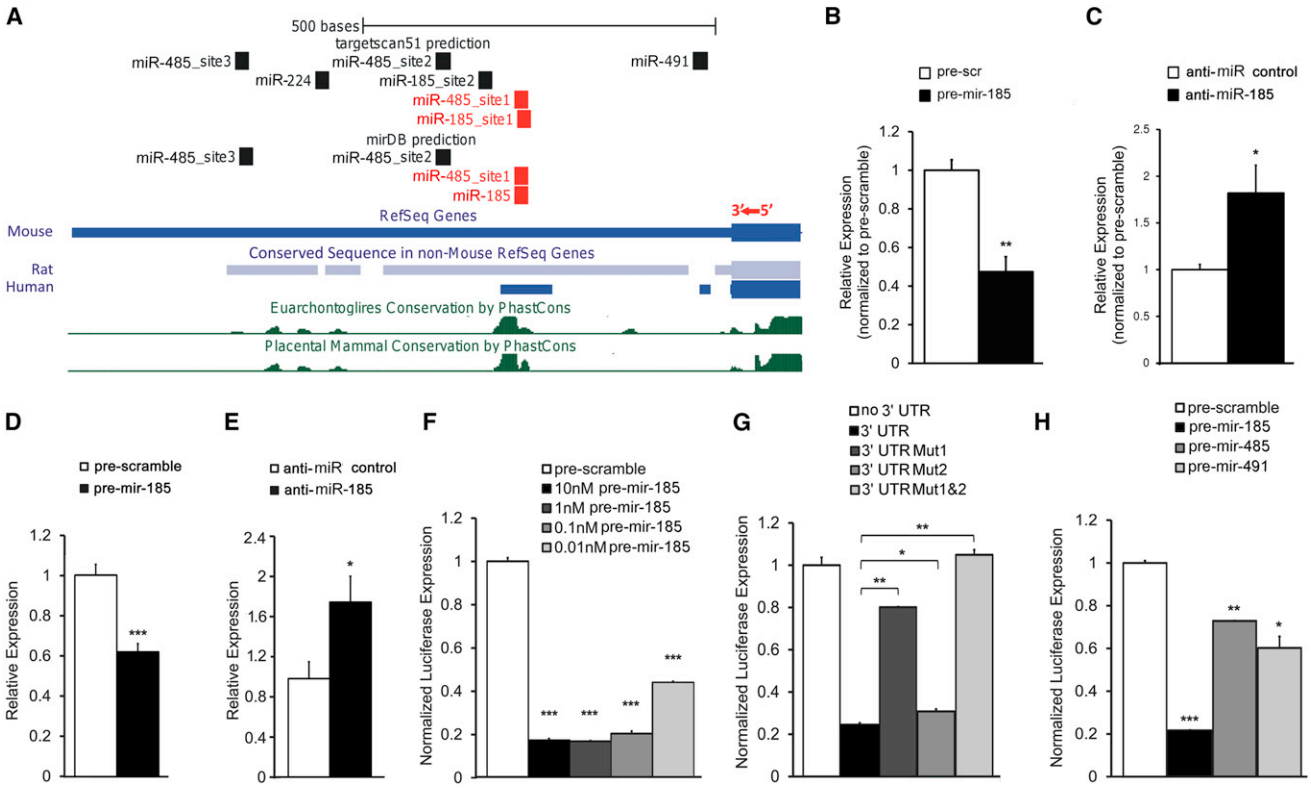

Figure 3. miR-185 Directly Targets and Represses *2310044H10Rik*

(A) Structure of the 3′ UTR of *2310044H10Rik* (*Mirta22*) showing miRNA binding sites predicted by TargetScan or mirDB. Blocks in mouse *2310044H10Rik* (*Mirta22*) 3′ UTR that are highly conserved in rat and human orthologs are shown below the mouse 3′ UTR. Evolutionary conservation is also assessed by the "30-way multiz alignment and conservation analysis" in the USCS browser, with conserved blocks indicated by green peaks. miR-185 and miR-485 binding sites located within the conserved blocks are shown in red.

(B and C) qRT-PCR quantification of endogenous *2310044H10Rik* (*Mirta22*) in DIV7 hippocampal neurons. Expression levels in anti-miR-185-treated and pre-mir-185-treated neurons were normalized to expression levels under respective controls. (B) Increased expression levels of *Mirta22* in neurons transfected with anti-miR-185 at DIV5 (n = 5, each treatment). (C) Reduced expression levels of *Mirta22* in DIV9 hippocampal neurons transfected with pre-mir-185 mimic at DIV7 (n = 3, each treatment).

(D and E) qRT-PCR quantification of endogenous 2310044H10Rik (Mirta22) in N18 cells. Expression levels in pre-mir-185-treated and anti-miR-185-treated cells were normalized to expression levels under respective controls. (D) Reduced expression levels of *Mirta22* in cells transfected with pre-mir-185 mimic (n = 3, each treatment). (E) Upregulation of *Mirta22* in cells transfected with an anti-miR-185 LNA oligo (n = 3, each treatment).

(F–H) Repression effects of pre-mir-185, pre-mir-485, and pre-mir-491 on *Mirta22* 3′ UTR were examined by a dual-luciferase reporter assay (see Experimental Procedures). Values are *Renilla* luciferase levels relative to firefly luciferase levels and normalized to the relative expression levels under prescramble treatment (F and H) or to the relative expression levels from plasmid with no 3′ UTR (G) (n = 3 for each condition). Pre-mir-185 significantly decreases the *2310044H10Rik* (*Mirta22*) 3′ UTR reporter expression over a concentration range of 10–0.01 nM (F). Pre-mir-185-mediated repression on *2310044H10Rik* (*Mirta22*) 3′ UTR reporter expression depends on conserved miRNA binding sites (G). Pre-mir-485 and pre-mir-491 significantly decrease the *2310044H10Rik* (*Mirta22*) 3′ UTR reporter expression (H).

Results are expressed as mean ±SEM. *$p < 0.05$, **$p < 0.01$, and ***$p < 0.001$ (Student's t test). See also Figure S3 and Table S3.

($p < 0.05$), respectively (Figure 3G). Notably, the pre-mir-185 mimic could not repress luciferase activity driven from a mutant reporter where both binding sites are simultaneously disrupted (Figure 3G). Thus, both miR-185 cognate binding sites have an impact on the 3′ UTR-mediated regulation of *2310044H10Rik* expression, although the site disrupted in the Mut1 reporter (Site 1) seems to be the major target site via which miR-185 directly exerts its repressive effect.

We further addressed the dependence of *2310044H10Rik* 3′ UTR reporter repression on the levels of miR-485 or miR-491, which are also predicted to target binding sites in the 3′ UTR of the *2310044H10Rik* gene. Both of these miRNAs are modestly downregulated in the HPC of the *Df(16)A*$^{+/-}$ mice due to *Dgcr8* hemizygosity (Figure S3B). The pre-miRNA mimics of either miRNA modestly but significantly reduced the luciferase activity of the 3′ UTR-fused reporter compared to the prescramble control (pre-mir-485: 27%, $p < 0.05$; pre-mir-491: 35%, $p < 0.05$; Figure 3H). A three-factor ANOVA indicated that all three miRNAs (miR-185, miR-485, and miR-491) and their interactions have significant impact on the luciferase activity with the exception of the interaction between miR-485 and miR-491 (Table S3).

Taken together, these findings suggest that the persistent elevation of 2310044H10Rik levels observed in *Df(16)A*$^{+/-}$ mice is likely the result of the combined hemizygosity at *miR-185* and *Dgcr8* loci. Although more than one miRNA contributes, the major effect is due to the dramatic downregulation of miR-185. Consistent with this notion and the less profound reduction of miR-185 in *Dgcr8*$^{+/-}$ mice (Figure 1E), *2310044H10Rik* is only modestly upregulated in this strain (Figure S3A). Interestingly, a comparison between the 3′ UTR of human and mouse orthologs (Figure 3A) reveals that miR-185 cognate Site 1 as well as one miR-485 binding site are located within a highly conserved region, suggesting that these sites are critical in regulating the levels of the human ortholog (*C19orf63*). Consistent with this expectation, introduction of pre-mir-185 into human 293T cells resulted in a significant decrease of endogenous *C19orf63* levels (Figure S3C). In addition, similar to the pattern observed in the mouse brain, expression of *C19orf63* decreases in infant brain as depicted in BrainSpan database (http://www.brainspan.org).

It is noteworthy that inspection of our gene expression data set as well as qRT-PCR analysis of a sample of eight high-likelihood miR-185 targets identified by more than one prediction program did not reveal any additional significant changes of transcript levels in the brains of *Df(16)A*$^{+/-}$ mice (Figure S3D). Furthermore, unlike *2310044H10Rik*, none of the other top upregulated protein-coding genes (shown in Figure 2B) are consistently altered in both HPC and frontal cortex of E17, P6, and adult *Df(16)A*$^{+/-}$ mice, and only one of them (*B3gat1*, see below) is predicted to contain miR-185 seed sites in its 3′ UTR. Overall, although additional downstream targets of miR-185 likely exist (see below), our analysis suggests that *2310044H10Rik* represents the major downstream effector of miR-185 and a major hub target of miRNA dysregulation due to the 22q11.2 microdeletion. Due to confirmed miRNA-mediated regulation, we renamed the gene *Mirta22* (*miR*NA *ta*rget of the *22*q11.2 microdeletion).

Mirta22 Encodes a Neuronal Protein Residing in the Golgi Apparatus

Mirta22 encodes a 28 kDa protein without any known sequence homology or functional domain (http://www.uniprot.org/uniprot/Q3TAS6). The murine ortholog is located on mouse chromosome 7 and contains seven coding exons. The human ortholog (*C19orf63*) is located on chromosome 19q13.33 and encodes a protein with 92.3% identity to the murine protein (Figure 4A). One mouse reference sequence (isoform 1) is reported in GenBank, whereas two *C19orf63* isoforms (isoform 1 and 2) are reported in GenBank and in the literature (Junes-Gill et al., 2011). The protein encoded by isoform 1 is predicted to contain a N-terminal signal peptide, as well as a transmembrane segment (Figure 4A, red rectangles), which separates a long N-terminal region from a short C-terminal segment that contains a polyglycine tail with unknown function. Isoform 2 differs from isoform 1 by an alternatively spliced exon located after exon 6. The protein encoded by isoform 2 is shorter by eight amino acids, contains the N-terminal signal peptide but not the transmembrane segment, and is predicted to be secreted (Figure 4A). We raised a polyclonal antibody against a segment of the protein that is conserved in the mouse and human orthologs (amino acids 207–226, Figure 4A, green rectangle; see Extended Experimental Procedures; Figure S4). We validated the specificity of the antibody using a number of assays (see Extended Experimental Procedures; Figures S4A–S4C) and showed that it can also detect the secreted form of the protein in 293T cell cultures (Figure S4D). Western blot assays of protein extracts from the brain of *Df(16)A*$^{+/-}$ mice and WT littermates showed the expected increase (25%) in Mirta22 levels in mutant mice (Figure 4B). A similar magnitude increase of the Mirta22 immunocytochemical signal was observed in *Df(16)A*$^{+/-}$ cultured neurons, as compared to WT neurons (Figure 4C).

Immunostaining of neuronal cultures showed that Mirta22 is primarily a neuronal protein (Figure 4D, top). At the subcellular level, it is found primarily in the soma, where it colocalizes with the Golgi apparatus marker GM130 (Nakamura et al., 1995). As the neurons mature, it is also found in vesicles and tubular-like clusters within the dendritic shafts (Figure 4D, middle). Mirta22 immunoreactivity was not detected in cultures stained with preimmune serum (Figure S4E) and was diminished by 64% in *Mirta22* shRNA-transfected neurons (Figures S4F and S4G, lower panel). Immunohistochemical analysis demonstrated that Mirta22 is widely distributed in the brain, where it is localized in neurons (Figure 4D, bottom).

miR-185 Reduction Results in Coordinated Mild Dysregulation of Golgi-Related Genes

Accumulating evidence suggests that miRNAs may target functionally connected genes, often in a developmental stage-specific manner (Tsang et al., 2010; Zhang et al., 2009). Consistent with this notion, functional annotation clustering analysis of 2,695 out of 2,708 predicted miR-185 targets (TargetScan Mouse v.5.2) included in the DAVID *Mus musculus* gene functional annotation database (http://david.abcc.ncifcrf.gov) identified as the top enriched gene cluster (gene count = 159, Enrichment Score = 8.56, FDR-corrected $p = 2 \times 10^{-9}$) the Gene Ontology (cellular component) term "Golgi apparatus" (Figure 5A). Gene set enrichment analysis (GSEA) on the 2,708 predicted miR-185 targets ranked based on the gene expression profile of *Df(16)A*$^{+/-}$ mice also indicated that the Gene Ontology terms "Golgi apparatus part" and "Golgi apparatus" were among the top 20 gene sets in the adult HPC (Figure 5A). A global perspective on the enrichment of this miR-185 target gene set among the differentially expressed genes in the *Df(16)A*$^{+/-}$ mice showed a significant enrichment in the adult HPC expression profile ($p = 5 \times 10^{-4}$) where, as expected, most of the top genes were upregulated (n = 34), and only four genes were downregulated ($p < 0.005$, Figure 5B; Table S4). A considerably more modest enrichment was suggested for the E17 ($p = 0.02$) and P6 HPC ($p = 0.016$) profiles (Figure S5). Interestingly, there was no significant enrichment within the PFC profiles in any of the three ages tested (E17: $p = 0.6311$; P6: $p = 0.1326$; adult: $p = 0.244$). Expression changes were modest, with only 4 of 159 Golgi-related probe sets included among the top 100 in the adult HPC.

Altered miR-185 Levels Contribute to Structural Alterations of *Df(16)A*$^{+/-}$ Neurons

Df(16)A$^{+/-}$ mice show impaired formation of dendrites and spines in the HPC (Mukai et al., 2008) and the PFC (Figures

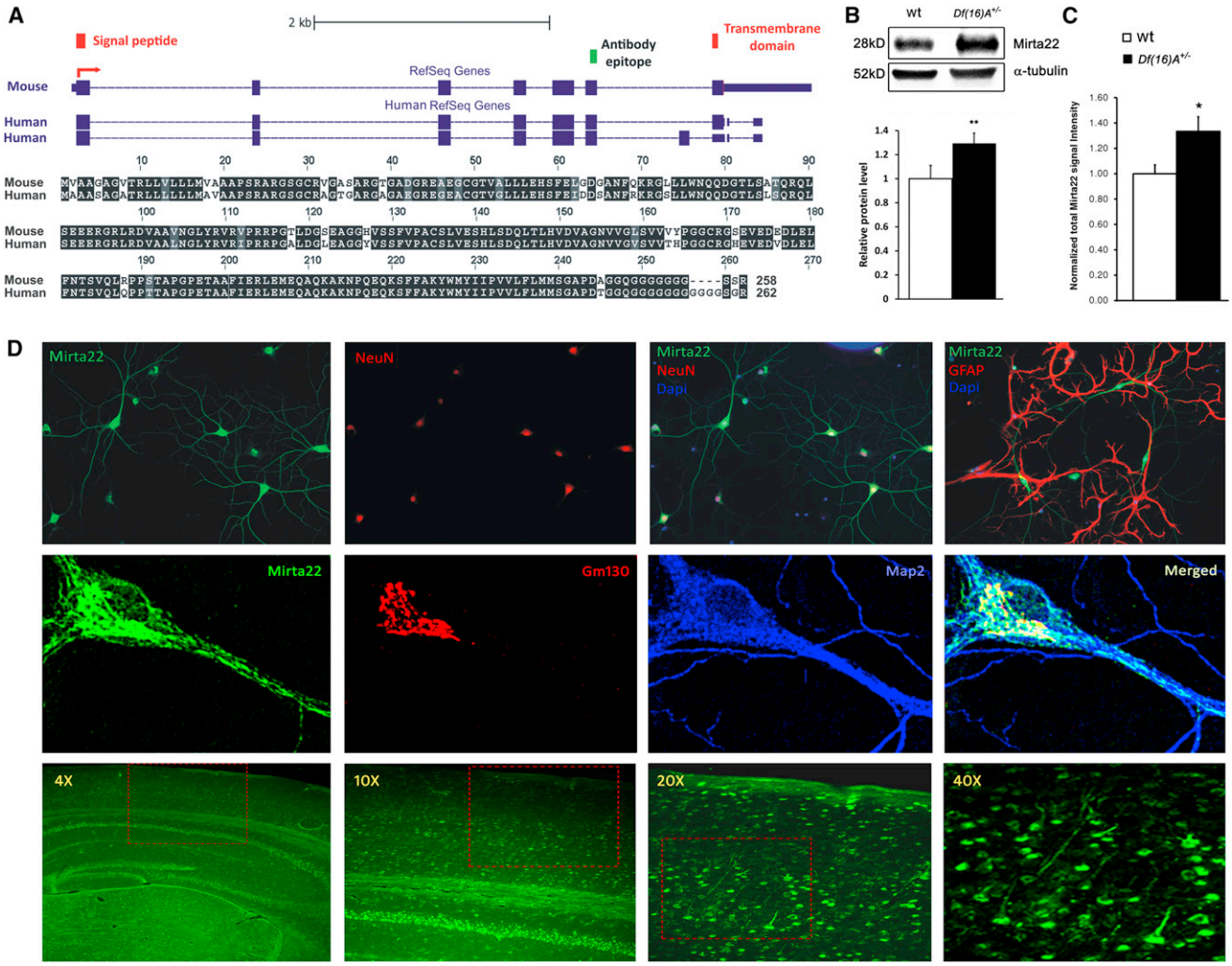

Figure 4. Genomic Structure, Neuronal Expression, and Subcellular Localization of 2310044H10Rik

(A) Top view shows the structure of mRNA transcripts of *2310044H10Rik* (*Mirta22*) and its human ortholog, *C19orf63*. RefSeq reports a *2310044H10Rik* (*Mirta22*) transcript with seven exons (blue rectangles), which is predicted to encode a signal peptide and a transmembrane domain (red rectangles). The peptide epitope used to generate a polyclonal antibody is marked by a green rectangle. For *C19orf63*, RefSeq reports two alternatively spliced transcripts: one that encodes a predicted transmembrane protein and one with an additional exon that encodes a predicted secreted protein. Bottom view shows protein sequence alignment of predicted transmembrane isoforms encoded by *2310044H10Rik* (*Mirta22*) and its human ortholog. Black blocks indicate completely conserved residues, gray blocks indicate similar residues (defined by Boxshade default similarities), and white blocks indicate different residues.

(B) Upper view presents representative western blot assays of 2310044H10Rik (Mirta22) in PFC lysates prepared from *Df(16)A*$^{+/-}$ animals and WT littermates. α-tubulin is used as loading control. Lower view is quantification of 2310044H10Rik (Mirta22) protein level in PFC of *Df(16)A*$^{+/-}$ and WT animals (n = 9 each genotype). Expression levels in mutant mice were normalized to WT littermates. Results are expressed as mean ±SEM. **$p < 0.01$ (Student's t test).

(C) Quantification of 2310044H10Rik (Mirta22) immunocytochemical signals in *Df(16)A*$^{+/-}$ and WT cultured neurons (n = 31 for *Df(16)A*$^{+/-}$; n = 34 for WT). Expression levels in mutant neurons were normalized to WT neurons. Results are expressed as mean ±SEM. *$p < 0.05$ (Student's t test).

(D) Upper panel shows that 2310044H10Rik (Mirta22) colocalizes with neuron-specific marker NeuN, but not with glia-specific marker GFAP, in cultured hippocampal neurons at DIV20. Middle panel shows that 2310044H10Rik (Mirta22) (green) colocalizes with Golgi-specific marker GM130 (red) in the soma. 2310044H10Rik (Mirta22) is also found in vesicles and tubular-like clusters in the dendrites, which are highlighted by the dendritic marker MAP2 (blue). Lower panel presents distribution of 2310044H10Rik (Mirta22) protein in adult mouse brain. Sections were stained with 2310044H10Rik (Mirta22) antibody. Images were taken at 4×, 10×, 20×, and 40× magnifications as indicated. Red boxes in 4×, 10×, and 20× images outline the area shown in 10×, 20×, and 40× images, respectively. See also Figure S4.

S6A–S6C), which are faithfully recapitulated in primary neuronal cultures. Impairment in these processes in *Df(16)A*$^{+/-}$ mice could only be partially accounted for by the 50% decrease in the levels of Dgcr8 (Fénelon et al., 2011; Stark et al., 2008). Localization of Mirta22 within the Golgi apparatus and dendritic shafts suggests that diminishment of the miR-185 repression on Mirta22 levels may also contribute to these deficits.

To test this hypothesis, we first asked whether reduction of miR-185 levels results in deficits in dendritic and spine development similar to those observed in *Df(16)A*$^{+/-}$ neurons (Mukai

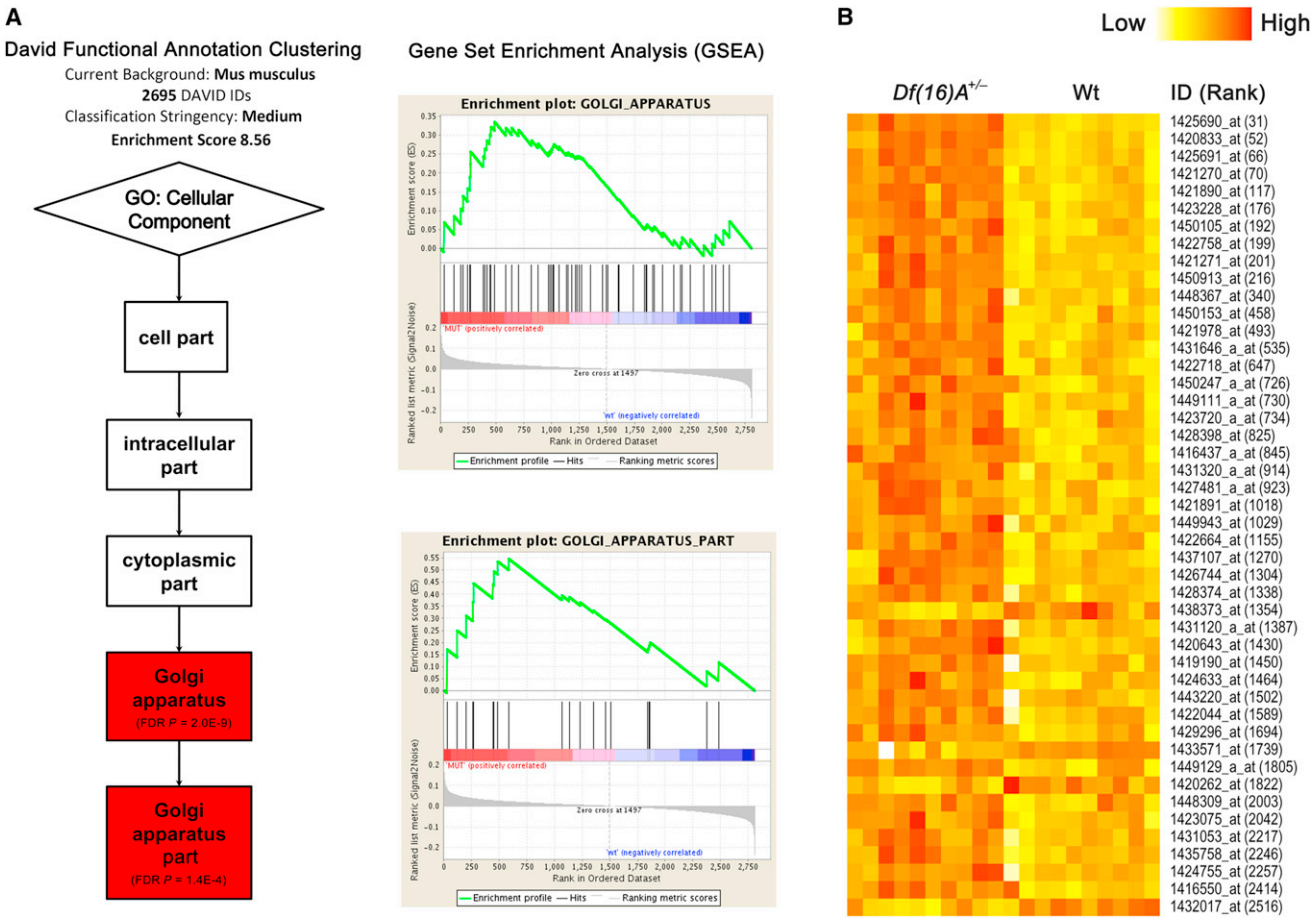

Figure 5. Coordinated Mild Dysregulation of Golgi-Related Putative miR-185 Targets in *Df(16)A*$^{+/-}$ Mice

(A) DAVID functional annotation clustering analysis (left) and GSEA (v.2.0) (right) of genes predicted as miR-185 targets by TargetScan Mouse v.5.2 identified Gene Ontology (GO) terms "Golgi apparatus" and "Golgi apparatus part" as the top enriched gene sets (see Extended Experimental Procedures).

(B) Expression heatmap plot of the potential miR-185 targets that serve Golgi apparatus-related functions (GO term) and are differentially expressed ($p < 0.005$) between adult HPC of *Df(16)A*$^{+/-}$ mice and WT littermates. ID, Affymetrix ID (see Table S4); Rank, the ranking position in the list of all differentially expressed genes according to significance level. Note that the majority (89%, 34 out of 38) of the genes are upregulated.

See also Figure S5 and Table S4.

et al., 2008). We introduced an anti-miR-185 and a scramble control LNA oligo into WT primary hippocampal neurons and measured dendritic and spine morphology 2 days posttransfection at DIV9 and DIV19, respectively. Analysis of dendritic architecture indicated that reduction of miR-185 levels leads to deficits in dendritic complexity (Figure 6A), including a significant reduction in the number of primary dendrites (21%, $p < 0.05$; Figure 6B) and a significant reduction in total branchpoints in transfected neurons (16%, $p < 0.05$; Figure 6C). This finding was confirmed by Sholl analysis, which compares branchpoint numbers at varying distances from the soma (Figure S6D). Moreover, reduction of miR-185 levels in DIV19 neurons results in decreased spine density (21%, $p < 0.05$; Figures 6D, 6E, and S6E) and a significant reduction in their median width (15% decrease, $p < 0.001$, Kolmogorov-Smirnov test; Figure 6F). Consistently, introduction of pre-mir-185 mimic into WT neurons increased the number of primary dendrites, number of branchpoints, density, and head width of mushroom spines (Figures S6F and S6G).

We also examined whether elevation of miR-185 levels could, at least partially, reverse cytoarchitectural alterations observed in *Df(16)A*$^{+/-}$ neurons (Mukai et al., 2008). We transfected primary hippocampal neurons from *Df(16)A*$^{+/-}$ mice and their WT littermates with pre-mir-185 or prescramble. A cotransfected GFP reporter plasmid allowed us to analyze the dendritic architecture (Figures 6G–6I) and spine morphology (Figures 6J–6L) of pyramidal neurons 2 days posttransfection at DIV9 and DIV19, respectively. Consistent with previous results (Mukai et al., 2008), compared to WT neurons, *Df(16)A*$^{+/-}$ neurons transfected with prescramble showed reduced dendritic complexity as manifested by a decrease in the number of primary dendrites (25%, $p < 10^{-10}$; Figure 6H) and number of dendritic branchpoints (38%, $p < 10^{-4}$; Figure 6I). They also showed reduced spine density (38%, $p < 10^{-6}$; Figure 6K) as well as a small but

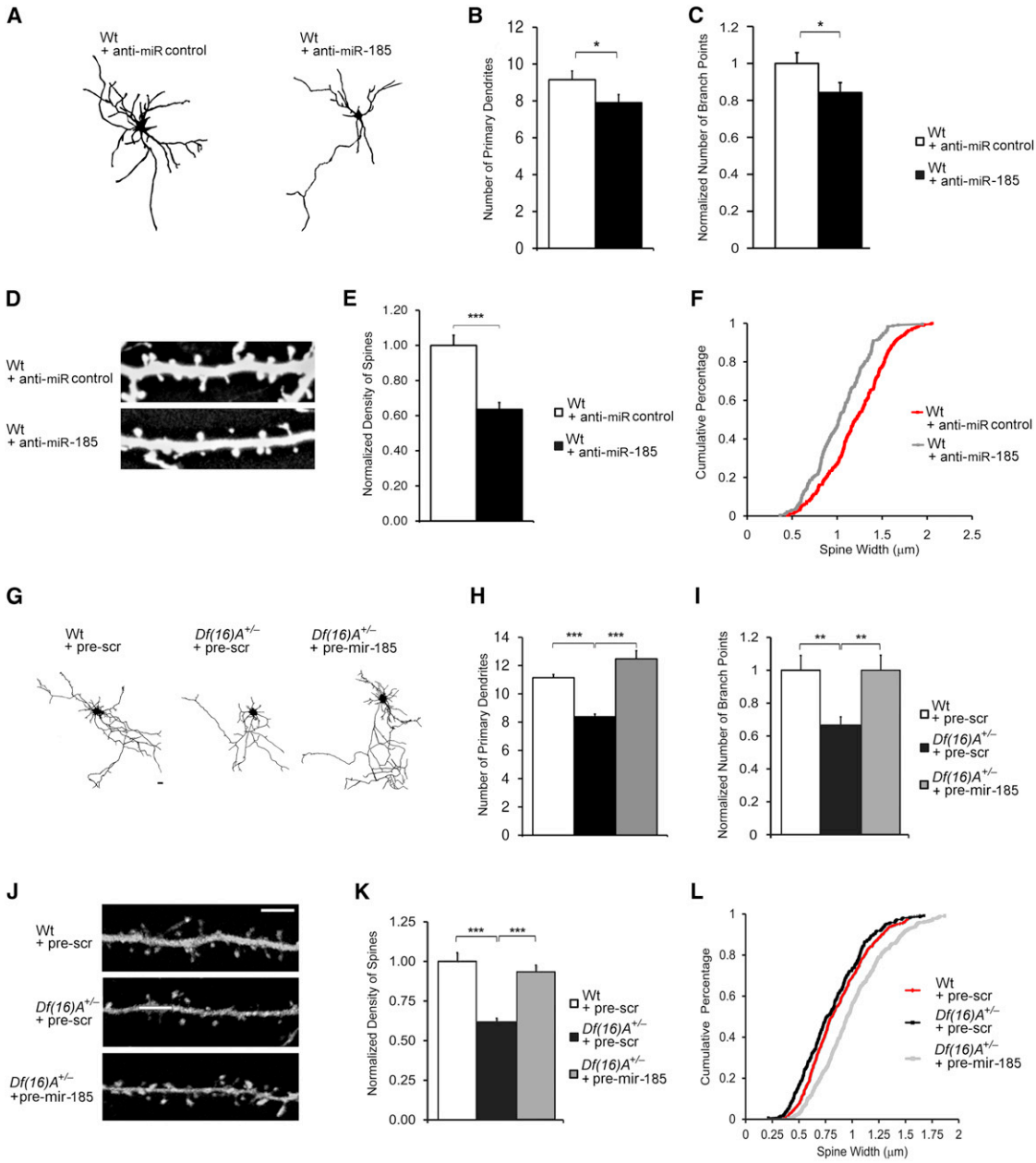

Figure 6. Reduced miR-185 Levels Contribute to Structural Alterations of *Df(16)A*$^{+/-}$ Neurons

(A) Representative images of WT neurons at DIV9 transfected with anti-miR control or anti-miR-185 oligos and enhanced GFP.

(B and C) Reduction in the number of primary dendrites (B) and branchpoints (C) in WT neurons at DIV9, 2 days after transfection with anti-miR-185 relative to WT neurons transfected with anti-miR control (n = 21 for WT + anti-miR-185; n = 20 for WT + anti-miR control). In (C), values of WT + anti-miR-185 were normalized to WT + anti-miR control.

(D) Representative images of spines on WT neurons at DIV19, transfected with anti-miR control or anti-miR-185, as well as enhanced GFP.

(E) Reduction in the density of mushroom spines in neurons transfected with anti-miR-185 relative to neurons transfected with anti-miR control (n = 20 for WT + anti-miR-185; n = 20 for WT + anti-miR control). Values of WT + anti-miR-185 were normalized to WT + anti-miR control.

(F) Transfection of anti-miR-185 oligos significantly decreased the width of mushroom spines compared to that of the neurons transfected with anti-miR control at DIV19 (15%, $p < 0.001$, Kolmogorov-Smirnov test) (n = 232 for WT + anti-miR-185; n = 293 for WT + anti-miR control).

(G) Representative *Df(16)A*$^{+/-}$ neurons at DIV9 transfected with prescramble or pre-mir-185 mimic and enhanced GFP for visualization. Scale Bar, 20 μm.

(H and I) Reduction in the number of primary dendrites (H) and branchpoints (I) in *Df(16)A*$^{+/-}$ neurons at DIV9 relative to WT neurons is reversed by the transfection of pre-mir-185, but not prescramble mimic (pre-scr) (n = 21 for WT + pre-scr; n = 21 for *Df(16)A*$^{+/-}$ + pre-scr; n = 21 for *Df(16)A*$^{+/-}$ + pre-mir-185). In (I), values of *Df(16)A*$^{+/-}$ neurons were normalized to WT + pre-scr.

(J) Representative images of spines on *Df(16)A*$^{+/-}$ neurons at DIV19, transfected with prescramble or pre-mir-185 mimic, as well as enhanced GFP. Scale Bar, 5 μm.

(legend continued on next page)

statistically significant decrease in median head width (8% decrease, $p < 0.01$; Figure 6L) of mushroom spines. Increase in miR-185 activity largely reversed the deficits in dendritic complexity (Figures 6H, 6I, and S6H) and the reduction in spine density (Figures 6K and S6I) and increased the head width of mushroom spines in *Df(16)A*$^{+/-}$ hippocampal neurons (Figure 6L).

Elevation of Mirta22 Levels Inhibits Dendritic and Spine Development in *Df(16)A*$^{+/-}$ Neurons

We examined whether elevation of Mirta22 levels could partially phenocopy the structural alterations observed in *Df(16)A*$^{+/-}$ neurons (Mukai et al., 2008). We introduced a *Mirta22* cDNA into WT primary hippocampal neurons and measured dendritic and spine morphology 2 days posttransfection, at DIV9 and DIV19, respectively. Control experiments using qRT-PCR and western blot confirmed that the *Mirta22*-encoding plasmid drives increased expression of *Mirta22* at both mRNA and protein levels (Figures S7A and S7B). Analysis of dendritic architecture indicated that elevation of Mirta22 levels results in a significant reduction in the number of primary dendrites (18%, $p < 0.001$; Figure S7C) and total branchpoints in transfected neurons (41%, $p < 10^{-5}$; Figure S7D). This finding was confirmed by Sholl analysis (Figure S7E). Moreover, elevation of Mirta22 levels in DIV19 neurons results in decreased spine density (22%, $p < 0.05$; Figure S7F) and a small but significant reduction in the mushroom spine median width (8% decrease, $p < 0.001$, Kolmogorov-Smirnov test; Figure S7G). These structural deficits recapitulate those observed in *Df(16)A*$^{+/-}$ neurons, suggesting that these deficits are, at least in part, due to the aberrantly high levels of Mirta22.

We also asked whether reduction of Mirta22 levels could, at least partially, reverse cytoarchitectural alterations observed in *Df(16)A*$^{+/-}$ neurons (Mukai et al., 2008). We transfected primary hippocampal neurons isolated from *Df(16)A*$^{+/-}$ embryos and their WT littermates with constructs that coexpress turbo RFP (tRFP) and either a shRNA engineered to knock down expression of endogenous mouse Mirta22 or a scramble control shRNA (scr shRNA). We confirmed that the *Mirta22* shRNA can effectively knock down the expression of *Mirta22* at both mRNA and protein levels (Figures S7H and S7I). We analyzed dendritic architecture and spine morphology 2 days following transfection, at DIV9 and DIV19, respectively. Introduction of *Mirta22* shRNA restored to WT levels the number of primary dendrites of *Df(16)A*$^{+/-}$ neurons at DIV9 (*Mirta22* shRNA versus scr shRNA, 40% increase, $p < 10^{-5}$; Figure 7A). A trend for increase in the total number of branchpoints in *Df(16)A*$^{+/-}$ neurons was also observed (25% increase, $p = 0.16$; Figure S7J). Sholl analysis confirmed that introduction of *Mirta22* shRNA in *Df(16)A*$^{+/-}$ neurons increased branchpoint numbers mainly in the proximal dendritic segments from the soma (Figure S7K). Furthermore, whereas DIV19 *Df(16)A*$^{+/-}$ neurons transfected with the control shRNA had fewer and thinner mushroom spines than WT neurons, introduction of *Mirta22* shRNA into *Df(16)A*$^{+/-}$ neurons reversed the deficit in density (*Mirta22* shRNA versus scr shRNA, 91% increase, $p < 10^{-6}$; Figure 7B), whereas it had no significant impact on spine width (Figure 7C). The observation that reduction of Mirta22 levels partially reverses the structural deficits observed in *Df(16)A*$^{+/-}$ mice was confirmed by using an independent *Mirta22* shRNA (Figures S7L–S7N) and strongly suggests that Mirta22 acts as an inhibitor mediating the effects of the structural mutation of dendritic and spine growth.

Reduction of Mirta22 Levels Reverses Structural Alterations in the HPC of *Df(16)A*$^{+/-}$ Mice

To determine whether *Mirta22* plays a role in vivo, we asked whether reduction of Mirta22 levels reverses previously reported deficits in dendritic and spine formation at hippocampal CA1 pyramidal neurons of *Df(16)A*$^{+/-}$ mice (Mukai et al., 2008). To this end, we used *Mirta22* mutant mice (2310044H10Rik$^{Gt(OST181617)Lex}$/Mmucd) carrying a retroviral gene trap insertion into intron 1 (Figure 7D). We confirmed that the insertion results in drastic reduction of *Mirta22* transcript and protein levels in the HPC of mutant mice (Figures 7E and 7F). We then crossed this line with *Df(16)A*$^{+/-}$ mice to generate mice compound heterozygous for the *Df(16)A* and *Mirta22* mutations (*Df(16)A*$^{+/-}$;*Mirta22*$^{+/-}$). Double mutants were compared to single mutants, as well as WT littermates, to evaluate the contribution of *Mirta22* upregulation to the dendritic and spine phenotypes induced by *Df(16)A*. We used diolistics to sparsely label individual HPC neurons with DiI and analyzed dendritic and spine morphology in the CA1 subfield of all four genotypes using confocal imaging.

Our analysis confirms previously reported alterations in complexity and spine formation at the basal dendritic tree of CA1 pyramidal neurons of *Df(16)A*$^{+/-}$ mice. Moreover, we show that the presence of the *Mirta22* mutation in compound heterozygous *Df(16)A*$^{+/-}$;*Mirta22*$^{+/-}$ mice reverses to WT levels the number of primary dendrites and total number of branchpoints (Figures 7G–7I). Sholl analysis confirmed that reduction of *Mirta22* levels in *Df(16)A*$^{+/-}$ mice results in increased dendritic branchpoint numbers (Figure 7J). Importantly, *Mirta22*$^{+/-}$ mice did not differ significantly from WT littermates in any of the tested parameters. Similarly, the presence of the *Mirta22* mutation in compound heterozygous *Df(16)A*$^{+/-}$;*Mirta22*$^{+/-}$ mice reversed to almost WT levels the *Df(16)A*-induced deficit in density and size of spines at the basal dendrites of CA1 neurons (Figures 7K–7M). *Mirta22*$^{+/-}$ mutants did not differ significantly from WT littermates in these two parameters.

(K) Reduction in the density of mushroom spines in DIV19 *Df(16)A*$^{+/-}$ neurons relative to WT control neurons is reversed by the transfection of pre-mir-185, but not prescramble mimic, into *Df(16)A*$^{+/-}$ neurons (n = 23 for WT + pre-scr; n = 21 for *Df(16)A*$^{+/-}$ + pre-scr; n = 23 for *Df(16)A*$^{+/-}$ + pre-mir-185). Values of *Df(16)A*$^{+/-}$ neurons were normalized to WT + pre-scr.

(L) Transfection of pre-mir-185 mimic, but not prescramble control, significantly increased the width of mushroom spines of *Df(16)A*$^{+/-}$ neurons at DIV19 (18%, $p < 0.001$, Kolmogorov-Smirnov test) (n = 568 for WT + pre-scr; n = 339 for *Df(16)A*$^{+/-}$ + pre-scr; n = 527 for *Df(16)A*$^{+/-}$ + pre-mir-185).

Results for (B), (C), (E), (H), (I), and (K) are expressed as mean ±SEM. *$p < 0.05$, **$p < 0.01$, ***$p < 0.001$ (Student's t test). See also Figure S6.

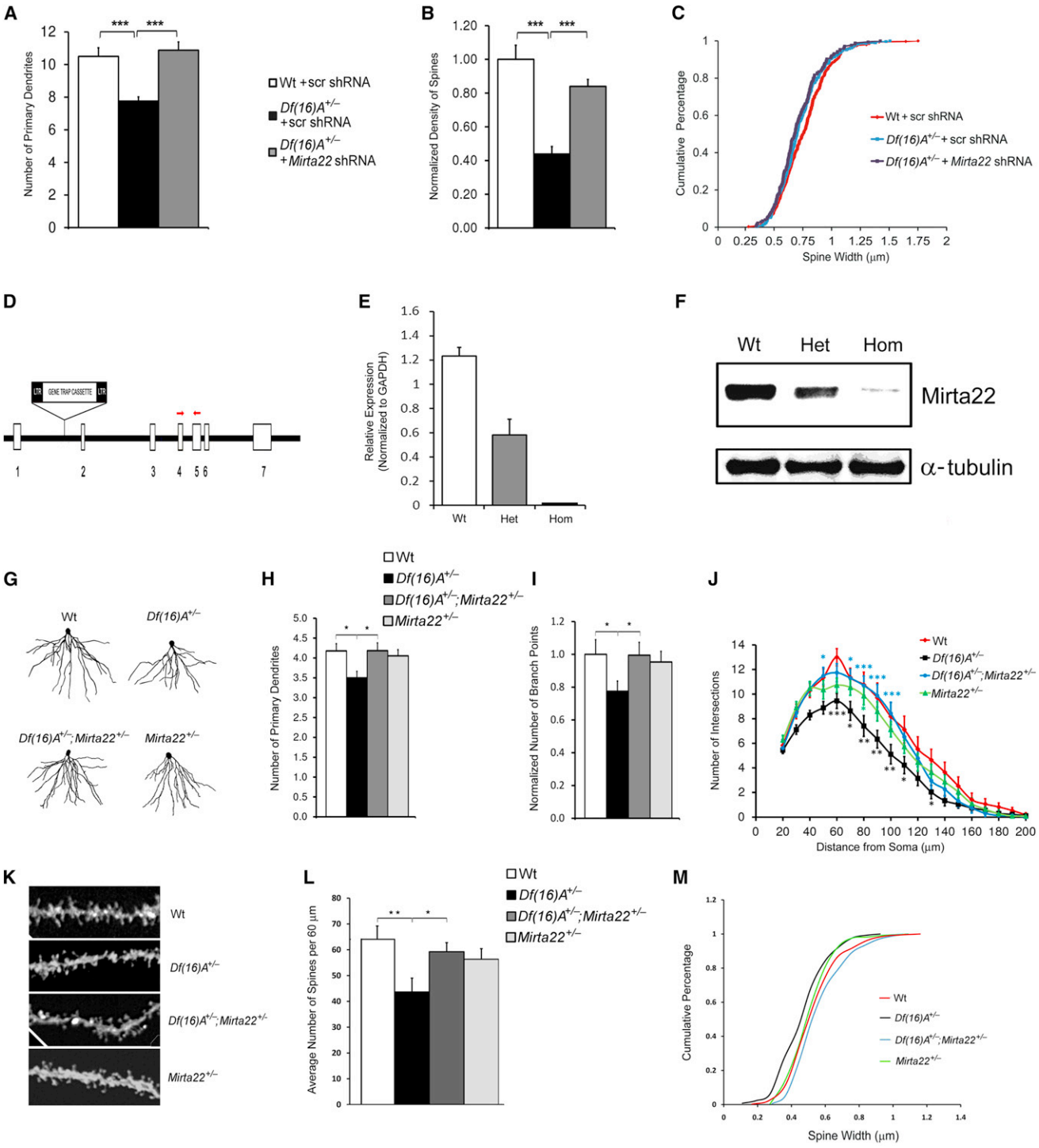

Figure 7. Reduction of *Mirta22* Levels Reverses Structural Alterations in the HPC of *Df(16)A*$^{+/-}$ Mice In Vitro and In Vivo

(A) Reduction in the number of primary dendrites in *Df(16)A*$^{+/-}$ neurons at DIV9 relative to WT neurons is reversed by the transfection of a construct that expresses *2310044H10Rik* (*Mirta22*) shRNA$^{+/-}$ (n = 24 for WT + scr shRNA; n = 21 for *Df(16)A*$^{+/-}$ + scr shRNA; n = 25 for *Df(16)A*$^{+/-}$ + *Mirta22* shRNA).

(B) Reduction in the density of mushroom spines in *Df(16)A*$^{+/-}$ neurons at DIV19 relative to WT neurons is reversed by the introduction of *Mirta22* shRNA, but not scr shRNA (n = 22 for WT + scr shRNA; n = 24 for *Df(16)A*$^{+/-}$ + scr shRNA; n = 15 for *Df(16)A*$^{+/-}$ + *Mirta22* shRNA). Values of *Df(16)A*$^{+/-}$ neurons were normalized to WT + scr shRNA.

(C) Transfection of *Mirta22* shRNA does not affect the width of mushroom spines of *Df(16)A*$^{+/-}$ neurons at DIV19 ($p > 0.05$, Kolmogorov-Smirnov test; n = 342 for WT + pre-scr; n = 289 for *Df(16)A*$^{+/-}$ + pre-scr; n = 177 for *Df(16)A*$^{+/-}$ + pre-mir-185).

(legend continued on next page)

DISCUSSION

Accumulating evidence suggests that miRNAs play an important role in the pathogenesis and pathophysiology of psychiatric disorders and cognitive dysfunction (Moreau et al., 2011; Stark et al., 2008; Xu et al., 2010). Here, we provide a comprehensive view of the pattern of miRNA dysregulation emerging due to 22q11.2 deletions, which is shaped by the combined effect of *miR-185* and *Dgcr8* hemizygosity. In this context, our results show a considerably greater reduction than the expected 50% decrease in the expression of a 22q11.2 gene, indicating that mechanisms other than simple haploinsufficiency could represent an important and previously unappreciated component of CNV pathogenicity. Along these lines, our results also raise the intriguing possibility that 22q11.2 microdeletions, by partially disabling the miRNA machinery, create a sensitized genetic background, which promotes the effects of deleterious mutations that affect the expression or activity of a subset of miRNAs (Ambros, 2010; Brenner et al., 2010).

By comparing gene expression profiles over three developmental stages and three levels of genomic dosage at the 22q11.2 locus, we identified elevated levels of a previously uncharacterized gene, *Mirta22*, as the most robust change in gene expression resulting from the 22q11.2 microdeletion, as well as the major downstream transcriptional effect of the 22q11.2-associated miRNA dysregulation. Localization of Mirta22 in the Golgi apparatus and in vesicle and tubular-like extensions in dendrites is consistent with a role in membrane and protein trafficking and secretion, which is necessary for establishment and maintenance of neuronal connections (Evans et al., 2011; Horton et al., 2005; McAllister, 2000; Rosso et al., 2005; Wayman et al., 2006). *Mirta22* is likely to act in concert with other genes within the 22q11.2 deletion (Karayiorgou et al., 2010), including the *Zdhhc8* palmitoyl-transferase, which is also located in the Golgi apparatus and modulates dendritic and spine development (Mukai et al., 2008). Moreover, although Mirta22 represents a major downstream effector of miR-185 dysregulation, our finding of a coordinated miR-185 targeting of Golgi-apparatus-related genes suggests that *Mirta22* upregulation may act, in an age- and brain region-specific manner, in concert with other modestly altered miR-185 targets to interfere with the Golgi-related processes required for neuronal maturation. Thus, our findings highlight a link between the Golgi apparatus and neuronal phenotypes associated with the 22q11.2 microdeletion.

Mirta22 bias toward prenatal expression suggests that this gene may play an important role in both restricting neural circuit formation prenatally, when embryonically generated neurons are still migrating and extending their axons, and in permitting neuronal maturation and synaptogenesis to unfold in the postnatal brain, after neurons have migrated to their final destinations. Consistent with the notion that miRNAs function predominantly as fine-tuning regulators of the expression levels of their targets (Baek et al., 2008; Selbach et al., 2008), miR-185 and to a lesser extent other miRNAs affected by the 22q11.2 deletion appear to restrict and optimize *Mirta22* expression, presumably to avoid excessive inhibition during the critical stage of postnatal synapse formation. Accordingly, sustained derepression of the gene due to genomic loss at the 22q11.2 locus may have an impact on the formation of neural circuits in early postnatal development, as well as on their maintenance during adulthood. Such structural changes could result in local and long-distance disruptions of neuronal communication (Fénelon et al., 2011; Sigurdsson et al., 2010), contributing to the cognitive dysfunction, psychiatric phenotypes, or both. In agreement with this prediction, expression of the human ortholog of *Mirta22* (*C19orf63*) declines in infant brains (Kang et al., 2011).

It has been shown that, during the transition between human fetal and infant development, a large number of genes reverse their direction of expression from an increase in the first two trimesters in utero to a decrease in the third trimester (which corresponds to postnatal development in rodents; Clancy et al., 2007) as well as after birth. Approximately 40% of them are predicted miRNA targets (Colantuoni et al., 2011; Xu et al.,

(D) Schematic (not to scale) of the genomic structure of *Mirta22* depicting the gene trap insertion in the intron between exons 1 and 2. Red arrowheads indicate approximate genomic location of PCR primers used for qRT-PCR.

(E) *Mirta22* transcript levels in HPC of adult homozygous (n = 3) and heterozygous (n = 3) *Mirta22* mutant mice as well as their WT littermates (n = 3), as assayed by qRT-PCR.

(F) Representative western blot assay depicting Mirta22 protein levels in HPC of adult homozygous (Hom; n = 3) and heterozygous (Het; n = 3) *Mirta22* mutant mice as well as their WT littermates. Levels of α-tubulin are shown as internal loading controls.

(G) Representative images from diolistic labeling of basal dendrites of CA1 pyramidal neurons from all four tested genotypes. Brains were dissected from 8-week-old littermate mice.

(H and I) Number of primary dendrites (H) and branchpoints (I) in the basal dendritic tree of CA1 pyramidal neurons from all four tested genotypes (n = 17 for WT; n = 29 for $Df(16)A^{+/-}$; n = 23 for $Df(16)A^{+/-}$;$Mirta22^{+/-}$; n = 22 for $Mirta22^{+/-}$). In (I), values of $Df(16)A^{+/-}$ and $Df(16)A^{+/-}$;$Mirta22^{+/-}$ neurons were normalized to WT neurons.

(J) Sholl analysis of basal dendrite complexity of CA1 pyramidal neurons using 10 μm concentric circles around the soma (n = 17 for WT; n = 29 for $Df(16)A^{+/-}$; n = 23 for $Df(16)A^{+/-}$;$Mirta22^{+/-}$; n = 22 for $Mirta22^{+/-}$). Note that the reduction in branching in $Df(16)A^{+/-}$ CA1 neurons is more prominent at the 50–100 μm range from soma as compared to WT neurons (black asterisks for WT versus $Df(16)A^{+/-}$ comparison), and it is reversed in the presence of the *Mirta22* mutation (blue asterisks for $Df(16)A^{+/-}$ versus $Df(16)A^{+/-}$;$Mirta22^{+/-}$ comparison).

(K) Representative images of spines at the basal dendrites of CA1 pyramidal neurons from all four tested genotypes. Brains were dissected from 8-week-old littermate mice.

(L) Density of total spines in the basal dendritic tree of CA1 pyramidal neurons from all four tested genotypes. Note that reduction in spine density in $Df(16)A^{+/-}$ CA1 neurons is reversed in the compound heterozygous $Df(16)A^{+/-}$;$Mirta22^{+/-}$ mice (n = 14 for WT; n = 6 for $Df(16)A^{+/-}$; n = 9 for $Df(16)A^{+/-}$;$Mirta22^{+/-}$; n = 9 for $Mirta22^{+/-}$).

(M) Width of mushroom spines (quantified over 60 μm of dendritic length) in the basal dendritic tree of CA1 pyramidal neurons from all four tested genotypes. Note that reduction in width is reversed in the compound heterozygous mice $Df(16)A^{+/-}$;$Mirta22^{+/-}$ ($p < 0.001$, Kolmogorov-Smirnov test).

Results are expressed as mean ±SEM. *$p < 0.05$, **$p < 0.01$, ***$p < 0.001$ (Student's t test). See also Figure S7.

2012). In that respect, *Mirta22* is one example of a disease-related gene representative of this type of transcriptional trajectory indicative of a miRNA-imposed temporal control over the sequential maturation of neurons, synapses, and circuits. Analysis of common variation in the vicinity of the human ortholog (Schizophrenia Psychiatric Genome-Wide Association Study (GWAS) Consortium, 2011) identified one SNP (rs10401266) 35 kb upstream of *C19orf63* in a presumptive regulatory region with nominally significant association with SCZ ($p = 5 \times 10^{-3}$). The impact of rare variants in *C19orf63* remains to be determined, but importantly, we recently provided evidence that rare de novo deleterious mutations in genes showing a prenatal expression bias and miRNA regulation similar to *Mirta22* are enriched in individuals with SCZ, especially those with prominent early prepsychotic, deviant behaviors (Gilman et al., 2012; Xu et al., 2012). Overall, understanding how *Mirta22* affects neuronal connectivity and eventually behavior and cognition is likely to provide more general insights into the contribution of miRNAs in psychiatric and neurodevelopmental disorders, illuminate the patterns of neural complexity underlying these disorders, and facilitate development of new treatments.

EXPERIMENTAL PROCEDURES

Mutant Mice

All animal protocols used in this study are approved by Columbia University IACUC. *Df(16)A*$^{+/-}$ and *Dgcr8*$^{+/-}$ mice have been described previously (Stark et al., 2008; Mukai et al., 2008) and have been backcrossed into C57BL/6J background for over ten generations. *Mirta22* mutant mice (*2310044H10Rik*$^{Gt(OST181617)Lex}$/Mmucd, referred to as *Mirta22*$^{+/-}$) were obtained from the Mutant Mouse Regional Resource Centers supported by NIH.

qRT-PCR and Expression Profiling

Total RNA was isolated by miRNeasy mini kit. qRT-PCR was performed as described previously (Stark et al., 2008). For expression profiling, cDNA was generated and exposed to the Affymetrix Mouse genome 430 2.0 array, which includes 45,000 probe sets from >34,000 well-characterized mouse genes. Data were obtained using GeneChip Analysis Software Microarray Suite version 5 and analyzed with limma package in the Bioconductor project (http://www.bioconductor.org). Details are provided in Extended Experimental Procedures.

Analysis of Dendritic Complexity and Spine Morphology

Dissected E17 hippocampal neurons were plated at 2×10^5 cells/ml in 6-well plates, cultured for 9–19 days, and transfected with GFP or RFP plasmids depending on the experiment. CA1 pyramidal neurons were sparsely labeled using diolistic labeling (see Extended Experimental Procedures). Images of dendrites and dendritic spines were acquired as described previously by Mukai et al. (2008). An experimenter blind to the genotype performed imaging and analysis. Details are provided in Extended Experimental Procedures.

Luciferase Assays

Mirta22 3′ UTR was cloned into psiCHECK2. Binding site mutant clones were generated by PCR-based mutagenesis. N18 neuroblastoma cells were transfected with various psiCHECK2 reporter constructs together with pre-mir-185 mimic or prescramble control unless mentioned otherwise, and luciferase assays were performed using the Promega Dual-Luciferase Reporter Assay System. All experiments were performed at least two times, and all data presented are the average of three technical repeats. Details are provided in Extended Experimental Procedures.

Functional Enrichment Analysis of Predicted *miR-185* Targets

miR-185 target gene list was imported into DAVID gene functional annotation database. Functional annotation was conducted using the program's functional annotation clustering analysis with default settings. GSEA was conducted using GSEA v.2.0. Details are provided in Extended Experimental Procedures.

Antibodies

A 20 amino acid peptide ([C]-CEQAQKAKNPQEQKSFFAKY-[N]) was used to generate a rabbit polyclonal antibody. Western blot, immunohistochemistry, and immunocytochemistry assays were conducted as previously described (Mukai et al., 2008; Stark et al., 2008). Details are provided in Extended Experimental Procedures.

ACCESSION NUMBERS

Expression profiling data are available at Gene Expression Omnibus under accession number GSE29767.

SUPPLEMENTAL INFORMATION

Supplemental Information includes Extended Experimental Procedures, seven figures, and four tables and can be found with this article online at http://dx.doi.org/10.1016/j.cell.2012.11.052.

ACKNOWLEDGMENTS

We thank Yan Sun, Merilee Teylan, Xuanyi Zou, and Megan Sribour for support with the maintenance of the mouse colony and technical assistance. We are also grateful to Drs. David Sulzer and Guomei Tang for their kind help with the diolistic assays. We thank Drs. Jun Mukai and Mirna Kvajo for help and insights with the immunocytochemistry assays. We also thank Dr. Mirna Kvajo and Rebbeca Levy for critical reading of the manuscript. This work was supported by a grant from the Simons Foundation (to J.A.G.), US National Institute of Mental Health grants MH67068 (to M.K. and J.A.G.), MH077235, and MH97879 (to J.A.G.), and by grants from the March of Dimes Foundation and the McKnight Endowment Fund for Neuroscience (to M.K.). B.X. was supported in part by a National Alliance for Research on Schizophrenia and Depression (NARSAD) Young Investigator Award. K.L.S. was supported by a NARSAD Suzanne and John Golden Young Investigator Award. B.X., P.-K.H., M.K., and J.A.G. designed the research; B.X. and P.-K.H. performed the experiments and analyzed the data; K.L.S. contributed to the generation of the mouse strains; M.K. and J.A.G. supervised experiments and data analysis; and B.X., P.-K.H., M.K., and J.A.G. wrote the paper.

Received: March 18, 2012
Revised: August 23, 2012
Accepted: November 26, 2012
Published: January 17, 2013

REFERENCES

Ambros, V. (2010). MicroRNAs: genetically sensitized worms reveal new secrets. Curr. Biol. *20*, R598–R600.

Arguello, P.A., and Gogos, J.A. (2006). Modeling madness in mice: one piece at a time. Neuron *52*, 179–196.

Arguello, P.A., and Gogos, J.A. (2010). Cognition in mouse models of schizophrenia susceptibility genes. Schizophr. Bull. *36*, 289–300.

Arguello, P.A., and Gogos, J.A. (2012). Genetic and cognitive windows into circuit mechanisms of psychiatric disease. Trends Neurosci. *35*, 3–13.

Baek, D., Villén, J., Shin, C., Camargo, F.D., Gygi, S.P., and Bartel, D.P. (2008). The impact of microRNAs on protein output. Nature *455*, 64–71.

Bearden, C.E., van Erp, T.G., Dutton, R.A., Lee, A.D., Simon, T.J., Cannon, T.D., Emanuel, B.S., McDonald-McGinn, D., Zackai, E.H., and Thompson, P.M. (2009). Alterations in midline cortical thickness and gyrification patterns mapped in children with 22q11.2 deletions. Cereb. Cortex *19*, 115–126.

Brenner, J.L., Jasiewicz, K.L., Fahley, A.F., Kemp, B.J., and Abbott, A.L. (2010). Loss of individual microRNAs causes mutant phenotypes in sensitized genetic backgrounds in C. elegans. Curr. Biol. *20*, 1321–1325.

Chahrour, M., Jung, S.Y., Shaw, C., Zhou, X., Wong, S.T., Qin, J., and Zoghbi, H.Y. (2008). MeCP2, a key contributor to neurological disease, activates and represses transcription. Science *320*, 1224–1229.

Chow, E.W., Zipursky, R.B., Mikulis, D.J., and Bassett, A.S. (2002). Structural brain abnormalities in patients with schizophrenia and 22q11 deletion syndrome. Biol. Psychiatry *51*, 208–215.

Clancy, B., Finlay, B.L., Darlington, R.B., and Anand, K.J. (2007). Extrapolating brain development from experimental species to humans. Neurotoxicology *28*, 931–937.

Colantuoni, C., Lipska, B.K., Ye, T., Hyde, T.M., Tao, R., Leek, J.T., Colantuoni, E.A., Elkahloun, A.G., Herman, M.M., Weinberger, D.R., and Kleinman, J.E. (2011). Temporal dynamics and genetic control of transcription in the human prefrontal cortex. Nature *478*, 519–523.

Evans, S.F., Irmady, K., Ostrow, K., Kim, T., Nykjaer, A., Saftig, P., Blobel, C., and Hempstead, B.L. (2011). Neuronal brain-derived neurotrophic factor is synthesized in excess, with levels regulated by sortilin-mediated trafficking and lysosomal degradation. J. Biol. Chem. *286*, 29556–29567.

Fénelon, K., Mukai, J., Xu, B., Hsu, P.K., Drew, L.J., Karayiorgou, M., Fischbach, G.D., Macdermott, A.B., and Gogos, J.A. (2011). Deficiency of Dgcr8, a gene disrupted by the 22q11.2 microdeletion, results in altered short-term plasticity in the prefrontal cortex. Proc. Natl. Acad. Sci. USA *108*, 4447–4452.

Fineberg, S.K., Kosik, K.S., and Davidson, B.L. (2009). MicroRNAs potentiate neural development. Neuron *64*, 303–309.

Gilman, S.R., Chang, J., Xu, B., Bawa, T.S., Gogos, J.A., Karayiorgou, M., and Vitkup, D. (2012). Diverse types of genetic variation converge on functional gene networks involved in schizophrenia. Nat. Neurosci. *15*, 1723–1728.

Grimson, A., Farh, K.K., Johnston, W.K., Garrett-Engele, P., Lim, L.P., and Bartel, D.P. (2007). MicroRNA targeting specificity in mammals: determinants beyond seed pairing. Mol. Cell *27*, 91–105.

Horton, A.C., Rácz, B., Monson, E.E., Lin, A.L., Weinberg, R.J., and Ehlers, M.D. (2005). Polarized secretory trafficking directs cargo for asymmetric dendrite growth and morphogenesis. Neuron *48*, 757–771.

International Schizophrenia Consortium. (2008). Rare chromosomal deletions and duplications increase risk of schizophrenia. Nature *455*, 237–241.

Junes-Gill, K.S., Gallaher, T.K., Gluzman-Poltorak, Z., Miller, J.D., Wheeler, C.J., Fan, X., and Basile, L.A. (2011). hHSS1: a novel secreted factor and suppressor of glioma growth located at chromosome 19q13.33. J. Neurooncol. *102*, 197–211.

Kang, H.J., Kawasawa, Y.I., Cheng, F., Zhu, Y., Xu, X., Li, M., Sousa, A.M., Pletikos, M., Meyer, K.A., Sedmak, G., et al. (2011). Spatio-temporal transcriptome of the human brain. Nature *478*, 483–489.

Karayiorgou, M., Morris, M.A., Morrow, B., Shprintzen, R.J., Goldberg, R., Borrow, J., Gos, A., Nestadt, G., Wolyniec, P.S., Lasseter, V.K., et al. (1995). Schizophrenia susceptibility associated with interstitial deletions of chromosome 22q11. Proc. Natl. Acad. Sci. USA *92*, 7612–7616.

Karayiorgou, M., Simon, T.J., and Gogos, J.A. (2010). 22q11.2 microdeletions: linking DNA structural variation to brain dysfunction and schizophrenia. Nat. Rev. Neurosci. *11*, 402–416.

Kosik, K.S. (2006). The neuronal microRNA system. Nat. Rev. Neurosci. *7*, 911–920.

McAllister, A.K. (2000). Cellular and molecular mechanisms of dendrite growth. Cereb. Cortex *10*, 963–973.

Moreau, M.P., Bruse, S.E., David-Rus, R., Buyske, S., and Brzustowicz, L.M. (2011). Altered microRNA expression profiles in postmortem brain samples from individuals with schizophrenia and bipolar disorder. Biol. Psychiatry *69*, 188–193.

Morrow, E.M. (2010). Genomic copy number variation in disorders of cognitive development. J. Am. Acad. Child Adolesc. Psychiatry *49*, 1091–1104.

Mukai, J., Dhilla, A., Drew, L.J., Stark, K.L., Cao, L., MacDermott, A.B., Karayiorgou, M., and Gogos, J.A. (2008). Palmitoylation-dependent neurodevelopmental deficits in a mouse model of 22q11 microdeletion. Nat. Neurosci. *11*, 1302–1310.

Nakamura, N., Rabouille, C., Watson, R., Nilsson, T., Hui, N., Slusarewicz, P., Kreis, T.E., and Warren, G. (1995). Characterization of a cis-Golgi matrix protein, GM130. J. Cell Biol. *131*, 1715–1726.

Rodriguez-Murillo, L., Gogos, J.A., and Karayiorgou, M. (2012). The genetic architecture of schizophrenia: new mutations and emerging paradigms. Annu. Rev. Med. *63*, 63–80.

Rosso, S.B., Sussman, D., Wynshaw-Boris, A., and Salinas, P.C. (2005). Wnt signaling through Dishevelled, Rac and JNK regulates dendritic development. Nat. Neurosci. *8*, 34–42.

Schizophrenia Psychiatric Genome-Wide Association Study (GWAS) Consortium. (2011). Genome-wide association study identifies five new schizophrenia loci. Nat. Genet. *43*, 969–976.

Schratt, G. (2009). microRNAs at the synapse. Nat. Rev. Neurosci. *10*, 842–849.

Selbach, M., Schwanhäusser, B., Thierfelder, N., Fang, Z., Khanin, R., and Rajewsky, N. (2008). Widespread changes in protein synthesis induced by microRNAs. Nature *455*, 58–63.

Sigurdsson, T., Stark, K.L., Karayiorgou, M., Gogos, J.A., and Gordon, J.A. (2010). Impaired hippocampal-prefrontal synchrony in a genetic mouse model of schizophrenia. Nature *464*, 763–767.

Stark, K.L., Xu, B., Bagchi, A., Lai, W.S., Liu, H., Hsu, R., Wan, X., Pavlidis, P., Mills, A.A., Karayiorgou, M., and Gogos, J.A. (2008). Altered brain microRNA biogenesis contributes to phenotypic deficits in a 22q11-deletion mouse model. Nat. Genet. *40*, 751–760.

Tomari, Y., and Zamore, P.D. (2005). MicroRNA biogenesis: drosha can't cut it without a partner. Curr. Biol. *15*, R61–R64.

Tsang, J.S., Ebert, M.S., and van Oudenaarden, A. (2010). Genome-wide dissection of microRNA functions and cotargeting networks using gene set signatures. Mol. Cell *38*, 140–153.

Wang, X. (2008). miRDB: a microRNA target prediction and functional annotation database with a wiki interface. RNA *14*, 1012–1017.

Wayman, G.A., Impey, S., Marks, D., Saneyoshi, T., Grant, W.F., Derkach, V., and Soderling, T.R. (2006). Activity-dependent dendritic arborization mediated by CaM-kinase I activation and enhanced CREB-dependent transcription of Wnt-2. Neuron *50*, 897–909.

Xu, B., Roos, J.L., Levy, S., van Rensburg, E.J., Gogos, J.A., and Karayiorgou, M. (2008). Strong association of de novo copy number mutations with sporadic schizophrenia. Nat. Genet. *40*, 880–885.

Xu, B., Karayiorgou, M., and Gogos, J.A. (2010). MicroRNAs in psychiatric and neurodevelopmental disorders. Brain Res. *1338*, 78–88.

Xu, B., Ionita-Laza, I., Roos, J.L., Boone, B., Woodrick, S., Sun, Y., Levy, S., Gogos, J.A., and Karayiorgou, M. (2012). De novo gene mutations highlight patterns of genetic and neural complexity in schizophrenia. Nat. Genet. *44*, 1365–1369.

Zhang, L., Hammell, M., Kudlow, B.A., Ambros, V., and Han, M. (2009). Systematic analysis of dynamic miRNA-target interactions during C. elegans development. Development *136*, 3043–3055.